The Indonesian Journal of Computer Science
www.ijcs.net
Volume 15, Issue 1, February 2026
https://doi.org/10.33022/ijcs.v15i1.5095

FCS-MPC Strategy with Region-Based Voltage Vector Selection and Kalman Filtering in Shunt Active Power Filters for Power Quality Enhancement

Hnin Ei Phyu[1], Wunna Swe[2]
hnineiphyu.dtve@gmail.com[1], swethunay@gmail.com[2]
[1,2] Department of Electrical Power Engineering, Myanmar

Article Information

Received : 1 Feb 2026
Revised : 27 Feb 2026
Accepted : 28 Feb 2026

Keywords

Finite control set MPC, Kalman filter, region-based vector selection, shunt active power filter.

Abstract

Power quality issues caused by nonlinear and unbalanced loads, such as harmonics, reactive power demand, and current imbalance, pose significant challenges in modern distribution networks. Shunt Active Power Filters (SAPFs) provide an effective solution, but their performance depends on advanced control strategies. This study proposes a hybrid approach that integrates Finite Control Set Model Predictive Control (FCS-MPC) with region-based voltage vector selection to achieve fast dynamic response and reduced switching losses. The grid voltage cycle is divided into six regions, with only four candidate vectors evaluated per region, minimizing computational complexity. A Kalman filter further enhances prediction accuracy by mitigating measurement noise and control delays. MATLAB/Simulink implementation on a low-voltage distribution network demonstrates effective harmonic suppression, balanced source currents, and robust performance under sudden load variations. Results confirm IEEE 519 compliance, ensuring practical and reliable power quality improvement in smart grids.

A. Introduction

Ensuring power quality has become a pressing challenge in modern smart grids, where reliable energy delivery must coexist with increasingly complex and nonlinear load demands. An unbalanced system arises when either the supply voltages are unequal or the load impedances differ. In low-voltage distribution networks, the main cause is unbalanced loads, since single-phase a.c. appliances dominate. Overloading of certain phases and unequal sharing of single-phase loads across a three-phase system create this imbalance. Moreover, load conditions can change suddenly due to the switching of household devices, industrial machinery, or nonlinear equipment such as rectifiers and inverters, further contributing to unbalanced operation. These factors lead to harmonic distortion, reactive power consumption, and current imbalance, degrading efficiency and accelerating the aging of sensitive equipment. Shunt Active Power Filters (SAPFs) have emerged as a proven solution, injecting compensating currents to suppress harmonics, balance source currents, and enhance overall grid performance [9],[10].

To maximize SAPF effectiveness, advanced control strategies have been explored. Model Predictive Control (MPC) has gained prominence for its ability to manage multivariable dynamics, incorporate system constraints, and adapt to nonlinear operating conditions [1]. A notable variant, Finite Control Set MPC (FCS-MPC), leverages the discrete switching states of Voltage Source Inverters (VSIs), eliminating modulation stages and enabling fast dynamic response with precise harmonic compensation [11]. Despite these advantages, FCS-MPC faces practical challenges: the need to evaluate all switching states at each sampling instant increases computational demand, while frequent switching across inverter legs raises losses and reduces efficiency [2].

To address these limitations, this study proposes a hybrid control approach that integrates FCS-MPC with region-based voltage vector selection [15]. By dividing the grid voltage cycle into six regions and restricting evaluation to four candidate vectors per region, computational complexity is reduced. Additionally, only two inverter legs switch at high frequency while the third remains clamped, lowering switching losses without sacrificing compensation performance. Robustness is further enhanced through Kalman filtering, which estimates source currents and PCC voltages under noisy and uncertain conditions, improving prediction accuracy and control reliability [6]. The proposed method aims to achieve efficient harmonic mitigation and current balancing under unbalanced nonlinear loads, while ensuring practical applicability in low-voltage distribution networks. The findings are expected to contribute to practical SAPF deployment in smart grids, ensuring compliance with IEEE standards and enhancing long-term reliability.

B. Model Predictive Control (MPC)

Model Predictive Control (MPC) is a flexible technique that predicts future system behavior using mathematical models and real-time feedback, then selects the optimal control action by minimizing a cost function that reflects performance goals and system constraints [17]. In power electronic converters, MPC has proven highly effective for enhancing dynamic response and operational adaptability. Model Predictive Control (MPC) strategies are typically categorized into

Continuous Control Set MPC (CCS-MPC), which uses modulation techniques to generate switching signals, and Finite Control Set MPC (FCS-MPC), which directly selects switching states without modulation. Continuous Control Set MPC (CCS-MPC) computes continuous control signals over a finite prediction horizon, but its computational demand often exceeds the short sampling intervals required in fast-switching converters [1]. In contrast, Finite Control Set MPC (FCS-MPC) reformulates the problem into a discrete framework, evaluating only a limited number of switching states, which enables real-time feasibility with reduced complexity [13]. Accurate modeling remains essential in both approaches, with observers such as Luenberger, extended state observers, and Kalman filters mitigating parameter uncertainties and measurement noise [6]. Discretization also influences prediction accuracy: Euler methods are simple but less precise, while exact discretization improves fidelity at a higher computational cost [16]. In practice, CCS-MPC offers smoother control but struggles with microsecond-level sampling, whereas FCS-MPC achieves a practical balance by exploiting discrete switching decisions, region-based logic, and efficient observers for robust converter performance [3].

FCS-MPC directly applies the optimal switching command to the inverter at each sampling instant [11]. As shown in Figure 1, the process involves measuring system variables, predicting future states with a discrete-time model, evaluating a cost function, and selecting the switching state that minimizes it [13]. The chosen state is then applied to the converter, and this cycle repeats continuously, ensuring real-time adaptation to load changes and grid disturbances.

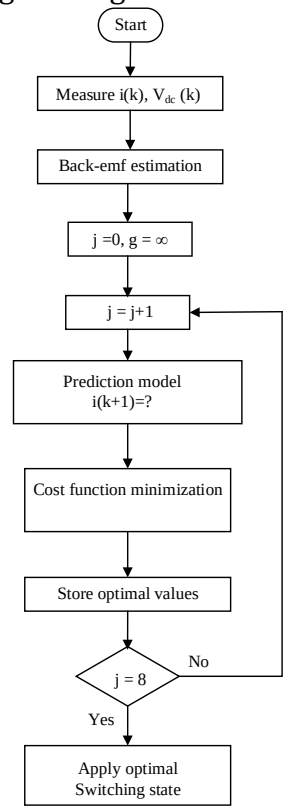

Figure 1. Flowchart of Optimal Switching Strategy

In FCS-MPC, the cost function drives the choice of optimal switching states [5]. Its primary role is to minimize the error between the reference and predicted currents. A quadratic form $g=(x^{*}-x)^2$ is commonly used, as it penalizes larger deviations more strongly and integrates well with predictive filtering such as Kalman estimation [8]. Extensions may include terms for switching effort, DC-link voltage deviation, or ripple minimization, with weights adjusted to balance accuracy, efficiency, and stability [12].

The effectiveness of MPC depends on three design parameters: sampling interval (T_s), prediction horizon (N_p), and weighting factors in the cost function [4]. Among these, T_s is most critical, as it governs discretization accuracy, stability, and responsiveness. In practice, computational delays introduce a one-sample lag, which is mitigated through delay compensation and observer-based estimation [14]. Kalman filtering enhances robustness by reducing measurement noise and providing one-step-ahead predictions [6]. Switching frequency is further regulated by penalizing control variations in the cost function, while region-based voltage vector selection minimizes losses by aligning inverter states with grid voltage polarity [9]. Together, these strategies enable precise harmonic suppression, reactive power compensation, and efficient real-time performance [16].

C. Control and Modelling Challenges in SAPF

A Shunt Active Power Filter (SAPF) typically consists of a voltage-source inverter (VSI) with a DC-link capacitor and AC-side inductors connected to the grid [9]. In three-wire systems without a neutral, the SAPF functions as a controllable current source, compensating reactive, harmonic, and unbalanced currents so that the grid experiences a balanced resistive load [11].

Designing effective SAPF control is challenging because the system must respond rapidly to nonlinear and unbalanced loads while minimizing switching losses [1]. Modeling difficulties arise from parameter variations, grid disturbances, and the nonlinear behavior of power converters, which complicate accurate prediction [4]. Control challenges include simultaneously achieving harmonic mitigation, balancing source currents and reducing computational burden [7].

Under noisy and uncertain operating conditions, disturbances further reduce accuracy and reliability [6]. Noise originates from sensor errors, switching ripple, electromagnetic interference, and digital quantization, while uncertainties stem from unpredictable load changes, imbalance, or drifting grid parameters due to aging, temperature, or voltage fluctuations [17]. These factors hinder real-time prediction and can degrade harmonic suppression and current balancing. To address this, observer-based methods such as the Kalman filter are employed to improve robustness by filtering measurement noise and enhancing state estimation [6].

D. Region-Based Vector Selection

Region-based control divides the grid voltage cycle into six 60° intervals. Within each region, only four voltage vectors are evaluated, rather than eight, reducing computational effort while maintaining dynamic accuracy [16]. This selective switching lowers losses and simplifies transitions without degrading harmonic performance [9].

Figure 2 illustrates the sinusoidal waveforms of a balanced three-phase grid voltage, segmented into six 60° intervals [12]. Each region highlights a unique combination of phase voltage polarities, guiding selective switching strategies. The phase offset ensures that two voltages share the same polarity while the third differs, forming the basis for region-based control.

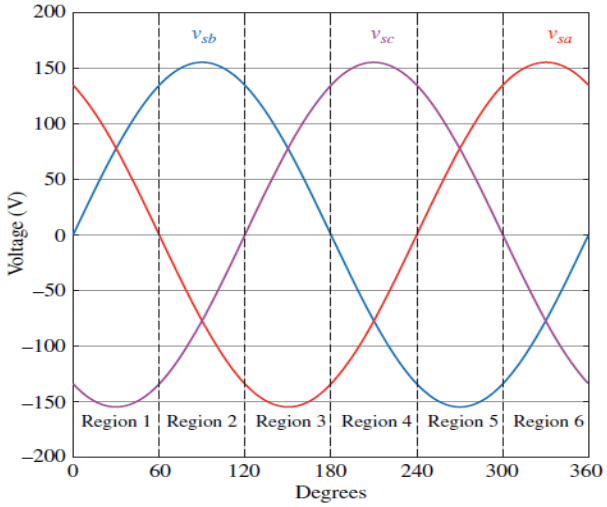

Figure 2. Three-Phase Grid Voltage Divided into Six Regions

Table 1 maps the inverter switching states (S_a, S_b, S_c) to corresponding voltage vectors (V_0 to V_7) [11]. Each binary combination represents a distinct output condition, enabling precise control of the active power filter. The structure simplifies modulation logic and supports efficient vector selection during operation.

Table 1. Switching states and voltage vectors

S_a	S_b	S_c	V_{apf}
0	0	0	V_0
1	0	0	V_1
1	1	0	V_2
0	1	0	V_3
0	1	1	V_4
0	0	1	V_5
1	0	1	V_6
1	1	1	V_7

Figure 3 partitions the control space into six directional regions, each linked to a binary-coded vertex (v_1 to v_6) [16]. Within each region, a sign-based vector (e.g., (+ + −), (− − +)) defines the modulation polarity of the three phases. The binary vertex labels represent switching states, guiding the selection of active voltage vectors. This structured layout supports efficient region-based control by aligning vector directionality with phase polarity transitions.

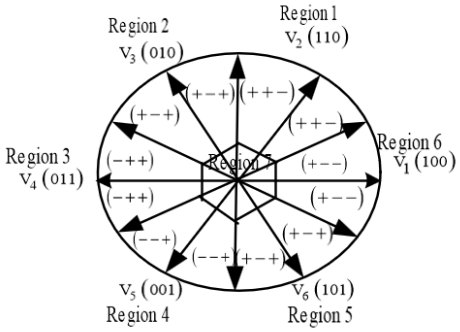

Figure 3. Hexa-Region Vector Assignment

Table 2 outlines the preferred voltage vectors for each 60° region based on phase voltage signs and switching logic [15]. By fixing one leg and modulating the other two, only four vectors are considered per region. This targeted approach reduces switching complexity while preserving dynamic response and harmonic quality.

Table 2. Pre-selection of voltage vectors for each region.

Region	v_{sa}	v_{sb}	v_{sc}	S_a	S_b	S_c	v_{apf}
0 –60	+	+	–	×	×	0	V_0, V_1, V_2, V_3
60 –120	–	+	–	×	1	×	V_2, V_3, V_4, V_7
120 –180	–	+	+	0	×	×	V_0, V_3, V_4, V_5
180 –240	–	–	+	×	×	1	V_4, V_5, V_6, V_7
240 –300	+	–	+	×	0	×	V_0, V_1, V_5, V_7
300 -360	+	–	–	1	×	×	V_1, V_2, V_6, V_7

E. Delay Compensation with Kalman Filter Integration

Real-time FCS-MPC often suffers from computation-induced delays [14]. To counter this, delay-aware models and anticipatory estimation are applied. The Kalman Filter (KF) is adapted to use predicted measurements y(k+1), aligning control actions with the next sampling instant [6]. Effective tuning requires balancing process noise covariance (Q), measurement noise covariance (R), and initial error covariance (P_0). Larger Q values improve responsiveness but risk amplifying noise, while smaller values enforce smoother estimates. R reflects sensor reliability, and P_0 sets initial confidence [17]. The KF operates through prediction and correction: forecasting the next state using system dynamics, then updating with new measurements via the Kalman gain L(k) [15]. This recursive

cycle ensures accurate state estimation, enhancing robustness against noise and delays.

The Kalman gain L(k), defined in Equation (1), is computed at each time step to optimally blend the predicted state with the actual measurement by balancing the uncertainties in the model and sensor data. It balances the uncertainty in the prediction (from the model) and the measurement (from sensors).

The formula is:

$$L(k) = P^{-}(k)C^{T}\left(CP^{-}(k)C^{T} + R\right)^{-1} \quad (1)$$

where $P^{-}(k)$ is predicted error covariance, C is the measurement matrix and R is the measurement noise covariance. The filter operates in two stages: the measurement update**,** which refines the state estimate using Equations (2) and (3), and the time update, which projects the state and error covariance forward using Equations (4) and (5). Mathematically, the update steps are,

Measurement update:

$$\hat{x}(k) = \hat{x}^{-}(k) + L(k)\left(y(k) - C\hat{x}^{-}(k)\right) \quad (2)$$

$$P(k) = \left(I - L(k)C\right).P^{-}(k) \quad (3)$$

Time update:

$$\hat{x}^{-}(k+1) = A\hat{x}(k) + Bu(k) \quad (4)$$

$$P^{-}(k+1) = AP(k)A^{T} + Q \quad (5)$$

The Kalman Filter estimates the state of a dynamic system by cycling through two main steps: prediction and correction [6],[18]. At each time step k, the filter begins with the previous corrected state estimate x^(k−1). Using the system model, it predicts the next state x^⁻(k) via the time update equation:

$$x^{-}(k) = Ax^{}(k-1) + Bu(k-1) \quad (6)$$

where A is the state-transition matrix and Bu(k−1) denotes the control input. This predicted state reflects the system's expectation before incorporating new measurements. Predicted error covariance update equation:

$$P^{-}(k) = AP(k-1)A^{T} + Q \quad (7)$$

At each iteration, the process begins with the previous corrected state estimate x^(k−1). The predicted state x^⁻(k) is obtained through the time update Equation (6), while the predicted error covariance is updated via Equation (7). When a new measurement y(k) becomes available, the Kalman gain L(k) is applied to correct the state estimate and update the error covariance, as shown in Equations (2) and (3). This recursive cycle of prediction and correction ensures that the Kalman Filter continuously refines its estimates by integrating model-based forecasts with real-time measurements, as illustrated in Figure 4.

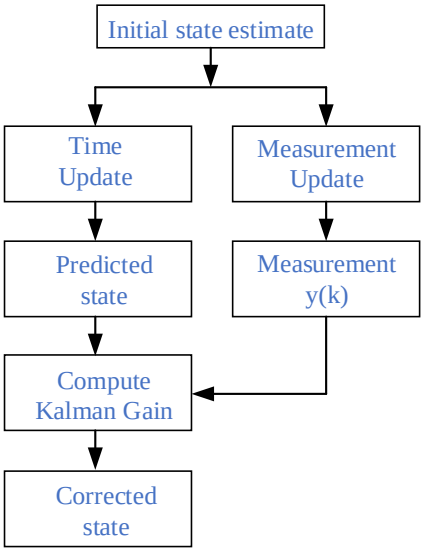

Figure 4. Block Diagram of the Kalman Filter Update Cycle

The Kalman Filter assimilation process, illustrated in Figure 5, follows a cyclical sequence of prediction and correction steps. Beginning with an initial state estimate, the algorithm generates a state prediction and evaluates the associated prediction error. The Kalman gain is then computed. Using this gain, the state estimate is corrected, and the correction error is assessed. If the assimilation is not yet complete, the process iterates. This iterative framework ensures that the final state estimate progressively converges toward the most accurate representation of the system.

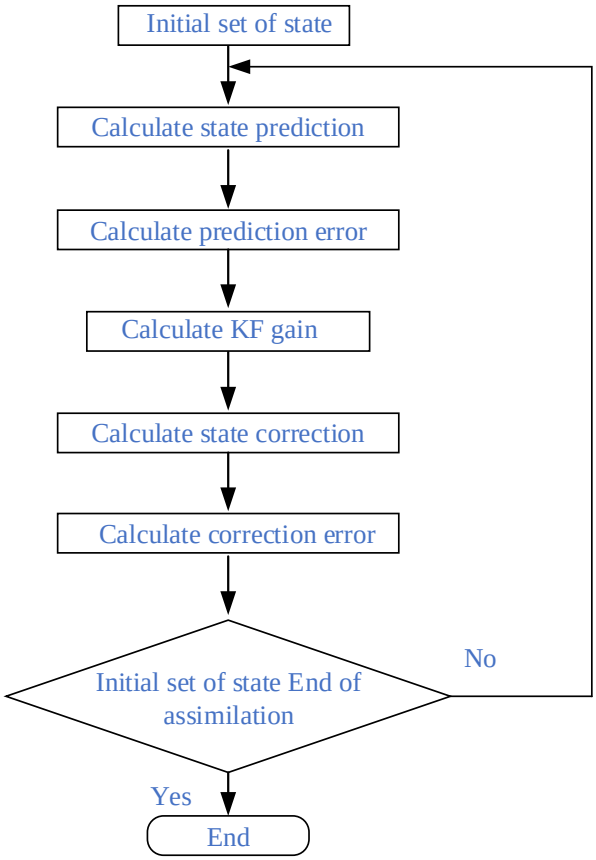

Figure 5. The Kalman Filter assimilation process

F. Results and Discussion

The proposed control strategy was implemented in MATLAB/Simulink to assess its effectiveness. A detailed simulation study was conducted on an 11/0.4 kV low-voltage distribution network, supplying nonlinear loads. To examine the transient performance of the SAPF, a sudden step increase in load current was introduced. This scenario provides a critical benchmark for evaluating the SAPF's compensation capability during abrupt disturbances. The THD of grid currents was used as the primary metric for harmonic suppression. Results confirm that the SAPF maintains stability and effectively compensates for nonlinear load effects. Figure 6 presents the structure of a Shunt Active Power Filter (SAPF) managed by Finite Control Set Model Predictive Control (FCS-MPC). The control unit predicts system behavior using real-time voltage and current feedback, selecting the best switching state for the Voltage Source Inverter (VSI) to reduce current error and harmonics. An RL filter smooths the inverter output, while the SAPF compensates for distortions caused by the nonlinear, unbalanced load.

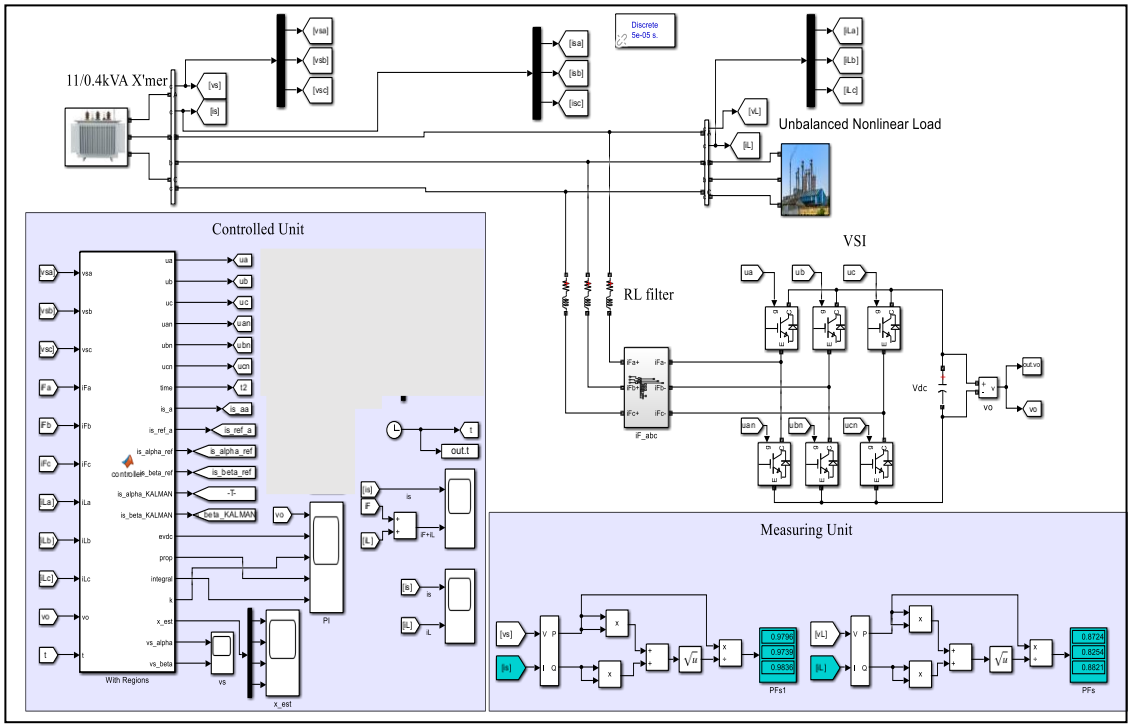

Figure 6. SAPF System Architecture with FCS-MPC Control

As shown in Figure 7, the nonlinear load produces three-phase currents (iL) that are distorted due to harmonic components. This figure illustrates that each phase has a distinct distortion and unequal load demand. In contrast, the source currents (is) remain balanced and sinusoidal, clearly demonstrating the effective compensation achieved by the FCS-MPC Shunt Active Power Filter (SAPF). At around 0.15 s, when the load demand increases, the supply currents smoothly adapt to meet the requirement. For clarity, only the highest and lowest phase current waveforms are shown, which sufficiently demonstrate the contrast between distorted and unbalanced load behavior and the effective real-time compensation achieved by the proposed control strategy.

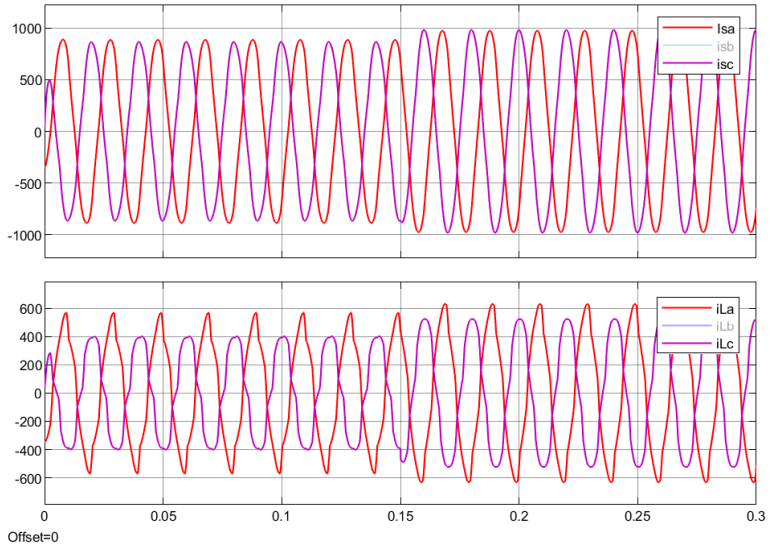

Figure 7. Balanced source currents adapt despite distorted load demand changes

Figure 8 shows the system's dynamic response under FCS-MPC control. The load currents (iLa,iLb,iLc) start distorted and unbalanced, then shift to higher amplitude around 0.2 s due to a load change. The SAPF adapts instantly, keeping source currents clean and stable, demonstrating real-time harmonic suppression and reliable supply current quality.

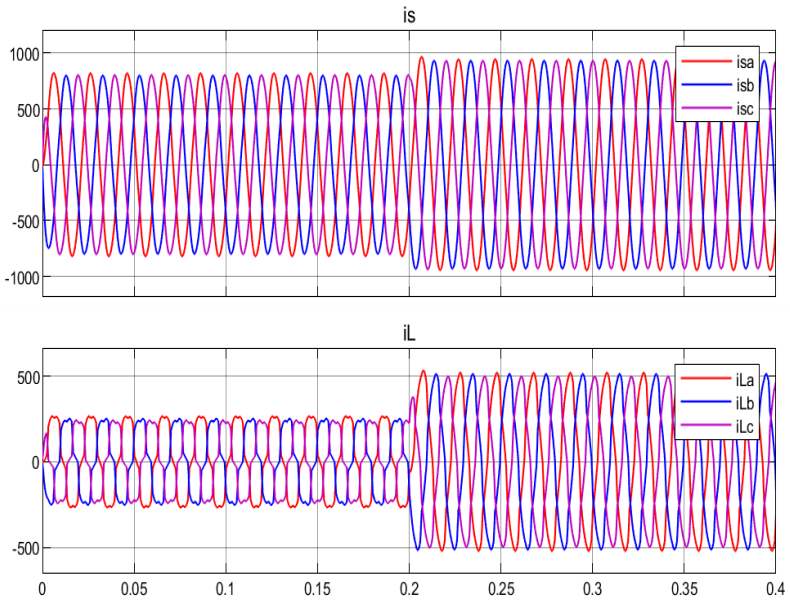

Figure 8. Source currents adapting under rising load demand at 0.2 s

Figure 9 also presents phase current comparison waveforms under transient disturbance. At approximately 0.2 s, the phase 'a' current experiences a transient disturbance, likely caused by a load variation or switching event. Despite this dynamic condition, the currents remain balanced and sinusoidal, confirming

that the SAPF effectively suppresses harmonic propagation and preserves current symmetry in real time.

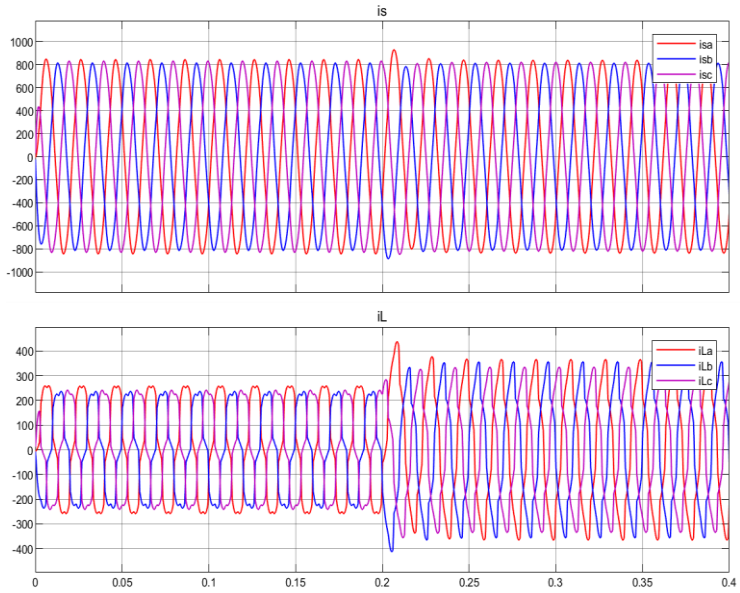

Figure 9. Phase current comparison waveforms with transient disturbance

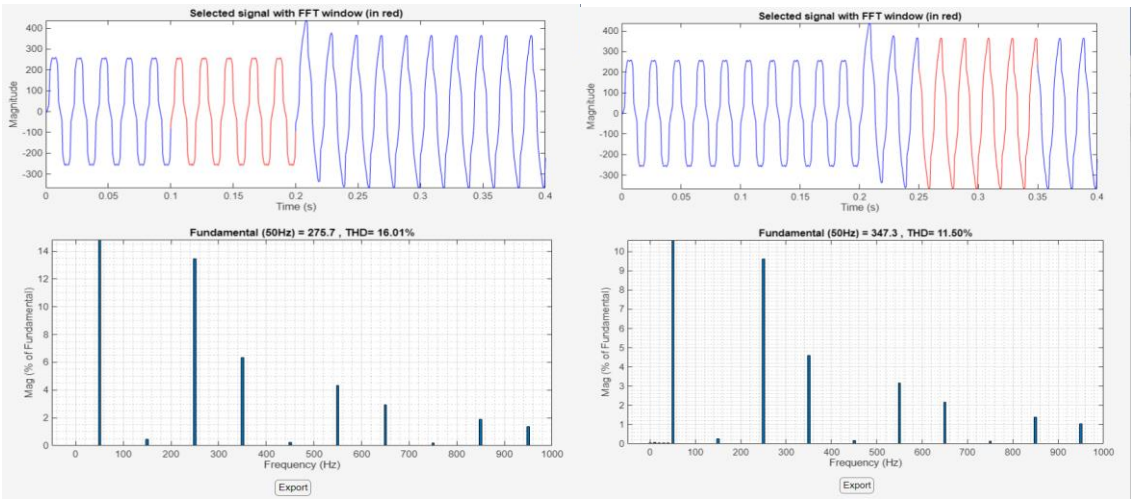

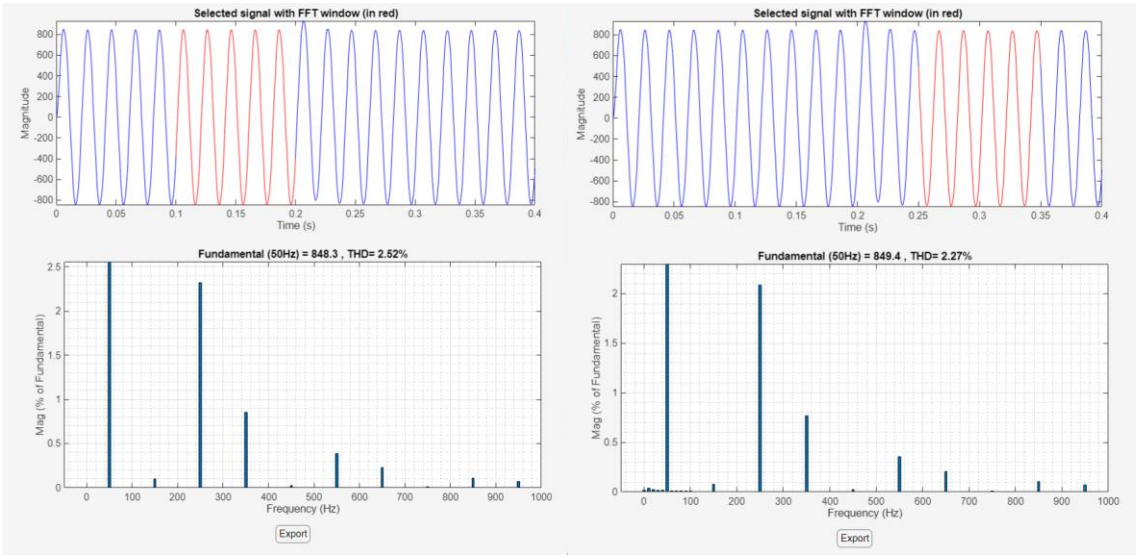

Figure 10. Phase 'a' source and load current THD% variation

Figure 10 compares the Total Harmonic Distortion (THD%) of phase 'a' currents under different load conditions. The source current initially shows higher distortion (THD% around 16% and 11%), while the compensated load current demonstrates much lower distortion (THD% around 2.5% and 2.3%).

Table 3. THD% Comparison Table

Figure No.	Phase	Before Load Changes		After Load Changes	
		Load Current THD%	Source Current THD%	Load Current THD%	Source Current THD%
2	a	9.43	3.11	7.09	2.44
	b	10.73	3.19	7.52	2.45
	c	11.91	3.35	7.83	2.51
3	a	16.45	2.22	6.78	1.43
	b	18..29	2.35	7.09	1.49
	c	18.71	2.3	7.21	1.47
4	a	16.01	2.52	11.5	2.27
	b	18.63	2.73	12.51	2.44
	c	17.8	2.59	12.7	2.34

Table 3 highlights how load and source current distortion levels change before and after load adjustments across different phases. Overall, the data shows a consistent reduction in source current THD%, indicating improved power quality. Across all figures, the nonlinear load introduces distortions and dynamic changes in three-phase currents, while the FCS-MPC SAPF consistently maintains balanced sinusoidal source currents. Step changes, load variations, and transient

disturbances are effectively compensated in real time, demonstrating harmonic suppression, current symmetry, and stable operation under challenging conditions. Simulation results further validate the approach with reduced THD, improved power factor, and reliable performance, confirming the hybrid FCS-MPC SAPF as a robust solution for real-time applications.

G. Conclusion

The proposed FCS-MPC Shunt Active Power Filter (SAPF) demonstrates strong capability in mitigating harmonics and maintaining balanced source currents under nonlinear and unbalanced load conditions. By incorporating a Kalman Filter, prediction accuracy is improved, while region-based voltage vector selection reduces computational complexity and switching losses. This layered control structure ensures fast dynamic response, reliable real-time operation, and enhanced power quality. The results confirm compliance with IEEE 519 standards and highlight the method's suitability for modern distribution networks where stability, efficiency, and robustness are critical.

H. References

[1] P. Karamanakos, "Model Predictive Control of Power Electronic Systems: Methods, Results, and Challenges," IEEE Open Journal of Industry Applications, vol. 1, pp. 1–17, Sep. 2020, doi: 10.1109/OJIA.2020.3020184.

[2] R. Kennel, J. Rodriguez, and Z. Zhang, "Model Predictive Control of Power Electronics – An Intuitive and Simple Concept for the Future," IEEE Industrial Electronics Magazine, vol. 17, no. 2, pp. 14–27, Jun. 2023, doi: 10.1109/MIE.2023.3267890.

[3] S. Borreggine, "A Review on Model Predictive Control and its Applications in Power Electronics," AEIT Journal of Power Electronics, vol. 2019, pp. xx–yy, 2019, ISBN: 9788887237436.

[4] M. Rivera, P. Karamanakos, and R. Guzmán, "Advanced Model Predictive Control Technologies for High-Power Applications," Energies, vol. 17, no. 4, pp. 2012, Feb. 2024, doi: 10.3390/en17042012.

[5] W. Gil-González, A. Escobar-Mejía, and O. D. Montoya-Giraldo, "Model Predictive Direct Power Control Applied to Grid-Connected Voltage Source Inverters," Energies, vol. 13, no. 21, pp. 1–18, Nov. 2020, doi: 10.3390/en13215567.

[6] R. Guzmán, J. M. Huerta, A. García-Cerrada, J. M. Rodríguez, and J. R. Torrealba, "Finite Control Set Model Predictive Control for a Three-Phase Shunt Active Power Filter with a Kalman Filter-Based Estimation," Energies, vol. 10, no. 10, pp. 1553, Oct. 2017, doi: 10.3390/en10101553.

[7] S. Vazquez, "Model Predictive Control: A Review of Its Applications in Power Electronics," IEEE Industrial Electronics Magazine, vol. 8, no. 1, pp. 16–31, Mar. 2014, doi: 10.1109/MIE.2013.2290138.

[8] J. M. E. Huerta, R. Guzmán, A. García-Cerrada, J. M. Rodríguez, and J. R. Torrealba, "A Synchronous Reference Frame Robust Predictive Current Control for Three-Phase Grid-Connected Inverters," IEEE Transactions on Industrial Electronics, vol. 57, no. 3, pp. 954–962, Mar. 2010.

[9] L. Tarisciotti, “Model Predictive Control for Shunt Active Filters With Fixed Switching Frequency,” IEEE Transactions on Industry Applications, vol. 53, no. 1, pp. 390–400, Jan./Feb. 2017.
[10] N. Mesbahi, “Model Predictive Control for Shunt Active Power Filter Under Both Balanced and Unbalanced Grid Conditions,” in Proc. IEEE Int. Conf. on Power Electronics and Applications, pp. 251–256, 2018, doi: 10.1109/PEA.2018.72810112.
[11] J. Rodriguez, P. Cortes, R. Kennel, M. P. Kazmierkowski, and D. E. Quevedo, “State of the Art of Finite Control Set Model Predictive Control in Power Electronics,” IEEE Transactions on Industrial Informatics, vol. 9, no. 2, pp. 1003–1016, May 2013, doi: 10.1109/TII.2012.2221469.
[12] T. H. Nguyen, R. Rabbeni, L. Tarisciotti, A. Formentini, P. Zanchetta, M. Pucci, and M. Rivera, “Finite Control Set–Model Predictive Control with Modulation to Mitigate Harmonic Component in Output Current for a Grid-Connected Inverter under Distorted Grid Conditions,” Energies, vol. 10, no. 7, pp. 907, Jul. 2017, doi: 10.3390/en10070907.
[13] H. E. Phyu and W. Swe, “Implementation of FCS-MPC Strategy in Shunt Active Power Filter for Power Quality Enhancement,” in Proc. Int. Conf. Adv. Electr. Electron. Eng. (ICAEEE), Indore, India, Jan. 2026.
[14] A. Formentini, L. Tarisciotti, and P. Zanchetta, “Recent Advances and Future Trends of Model Predictive Control in Power Electronics,” in Proc. IEEE IECON, pp. 1123–1130, Oct. 2025, doi: 10.1109/IECON.2025.10345678.
[15] A. Bemporad, “Model Predictive Control Design: New Trends and Tools,” in Proc. 45th IEEE Conf. Decision and Control (CDC), San Diego, CA, USA, pp. 6678–6683, 2006.
[16] R. Rabbeni, L. Tarisciotti, A. Gaeta, A. Formentini, P. Zanchetta, M. Pucci, M. Degano, and M. Rivera, “Finite States Modulated Model Predictive Control for Active Power Filtering Systems,” in Proc. IEEE Int. Conf. on Power Electronics and Applications, pp. 2510–2515, 2015.
[17] H. Komurcugil, S. Bayhan, R. Guzman, M. Malinowski, and H. Abu-Rub, Advanced Control of Power Converters: Techniques and Matlab/Simulink Implementation, IEEE Press Series on Control Systems Theory and Applications, Wiley-IEEE Press, Hoboken, NJ, 2023.
[18] J. Rodriguez and P. Cortes, Predictive Control of Power Converters and Electrical Drives, Wiley-IEEE Press, Chichester, UK, 2012.